LIDAR USING THE BACKSCATTER AMPLIFICATION EFFECT

Igor A. Razenkov*, Victor A. Banakh

*V.E. Zuev Institute of Atmospheric Optics, Tomsk, 634055, RUSSIA, *Email: lidaroff@iao.ru*

ABSTRACT

Experimental data proving the possibility of lidar measurement of the refractive turbulence strength based on the effect of backscatter amplification (BSA) are reported. It is shown that the values of the amplification factor correlate with the variance of random jitter of optical image of an incoherent light source depending on the value of the structure constant of the air refractive index turbulent fluctuations averaged over the probing path. This paper presents the results of measurements of the BSA factor in comparison with the simultaneous measurements of the BSA peak, which is very narrow and only occurs on the laser beam axis. It is constructed the range-time images of the derivative of the amplification factor gives a comprehensive picture of the location of turbulent zones and their temporal dynamics.

1. INTRODUCTION

It is known that, on double passage paths in random media, the mean intensity of the return optical wave in the strictly backward direction to the wave source can exceed the intensity of the wave reflected by a target in the same direction in a free space [1–4]. An increase of the mean intensity of the reflected wave in the strictly backward direction in random media as compared with that in a free space is referred to as the effect of backscatter amplification (BSA) [5-7]. This effect is caused by the correlation of the forward and backward waves traversing the same random inhomogeneities of the medium.

The BSA lidar is an aerosol micro pulse lidar (MPL) with one transmitting channel and two receiving (axial and off-axis) channels [8,9]. The axial receiving channel coincides with the transmitting channel. It records the echo signal in the direction of the axis of the probing beam. The receiving aperture of the off-axis channel is separated from the receiving aperture of the axial channel by the distance exceeding the correlation scale of intensity fluctuations in the probing beam. The ratio of the powers of lidar echo signals recorded in the axial and off-axis receiving channels determines the amplification *N*-factor [9].

This paper presents the results of measurements of the BSA factor in comparison with the simultaneous measurements of the variance of random jitter of optical image of an incoherent light source, whose value is directly proportional to the strength of refractive turbulence at the probing path. The results of scanning the BSA-peak and space-time mapping of the *N*-factor derivative are given.

2. LIDAR SETUP

The design of the lidar is shown schematically in Fig. 1. A laser beam 5 mm in diameter from fiber laser 1 (532 nm) is directed by mirror 2 to 50/50 beam splitter 3. After beam splitter 3, the beam is launched into the atmosphere through mirrors 4 and 5, afocal telescope 6-7, and round hole 9 (45 mm in diam.) in screen 8.

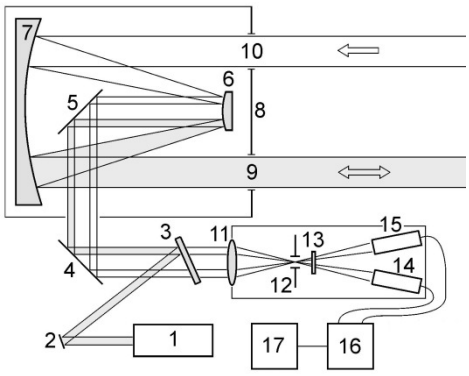

Fig. 1. Block diagram of the micro pulse BSA lidar.

The radiation backscattered in the atmosphere comes to the axial receiving channel through the same hole 9 in screen 8, the probing beam goes out. The backscattered radiation comes into the off-axis receiving channel through another hole 10 in screen 8, which is placed symmetric about the telescope axis.

After telescope 6-7, mirrors 5 and 4, and beam splitter 3, the scattered radiation of the axial and off-axis channels comes into the receiving box with a focusing lens 11 at an entrance. Aperture diaphragm 12 is set at a focus of lens 11. The diameter of this diaphragm determines the lidar field-of-view (350 μrad). The diaphragm is followed by interference filter 13 and PMT photo detectors of the axial 14 and off-axis 15 receiving channels. The repetition frequency of laser pulses with duration of 5 ns and energy of 10 μJ was 50 kHz. Accumulation time was 5 min, and the spatial resolution after averaging bins (1 bin =2 m) was 50 m.

For the additional experiment we used the third receiving channel served for recording of the profile of the backscatter amplification factor across the axial receiving channel [10]. For this purpose we set up beam-splitting plate (80/20) into the outgoing laser beam and small 10 mm objective was placed in the reflected incoming beam and installed on a computer-controlled movable platform. Platform allows one to scan the power distribution of the scattered radiation from hard target across the axial receiving channel. The use of the third receiving channel was possible only in the nighttime, when background noise was low.

3. EXPERIMENT

The experiment was conducted in Tomsk city at a 2-km path between two buildings 5 and 6 (Fig. 2). The measurements were carried out in winter time of 2016 at negative open-air temperatures. The BSA lidar operated continuously in the automatic mode. The recorded profiles of the amplification factor started at a distance of 800 m and ended at 1900 m. Simultaneously with measurements of the amplification factor, we measured the variance of arrival angles of the light wave from a white disk 80 mm in diameter on black 3 being at a distance of 2 km. For registration of the disk image a CCD camera with Maksutov objective was used. This additional setup is called as “image jitter sensor” (IJS). The focal length F of the objective was 1 m, and the diameter of the entrance aperture was D=100 mm. Objective 4 of the IJS was close to the axis of the transceiving telescope of lidar 1 at a 30 cm apart.

For the time of accumulation of the lidar signal (300 sec), the laser made 15 000 000 shots, and the receiver detected from hundred to several thousands of photons in every bin (13.3 ns) depending on the distance. The CCD camera recorded images with a frequency of 15 Hz. For the time of signal accumulation 4500 frames were recorded. During the measurement, the coordinates of energy centroid of the image of the white diffuse disk were determined for every frame in real time, and then the variances σ_y^2 and σ_z^2 of turbulence-induced random displacements of the energy centroid of the image along axes y and z were calculated.

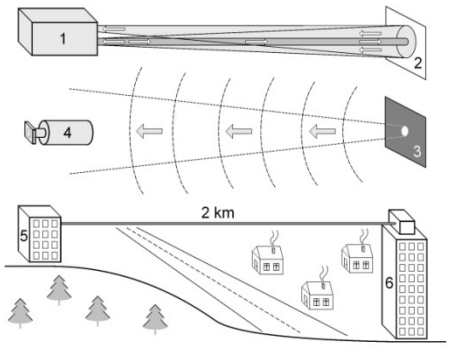

Fig. 2. Schematic of the experiment: lidar 1 and topographic target 2 (top), image jitter sensor: diffuse luminous white disk 3 on black and teleobjective with CCD camera 4 (center), probing path between buildings 5 and 6, and rough site plan (bottom).

4. BSA PEAK RESULTS

Based on the results [11], for the variance of random image jitter of an incoherent light source (diffuse disk) $\sigma_c^2 = \sigma_y^2 + \sigma_z^2$ we can obtain

$$\sigma_c^2 = c\, C_n^2\, D^{-\frac{1}{3}} L, \qquad (1)$$

where c is numerical constant, C_n^2 is the structure constant of turbulent fluctuations of the refractive index of air, L is the path length. In common case the variance of jitter σ_c^2 depends on the integral value of the air refractive index structure constant C_n^2 along the propagation path, and can be used for monitoring the refractive turbulence strength on the probing path.

Figure 3a shows the temporal profile of the amplification factor N at a distance of 1900 m. During this experiment was run the scanner operated continuously. Figure 3b depicts the value of the scanner signals for three scans within aria shown by double arrow on the Figure 3a, when the amplification factor was maximal. In all the scans,

we can clearly see the profile of the amplification factor in the cross section of the axial receiving channel. The position of the transceiver aperture ("beam") is shown by the horizontal bar in Fig. 3(b). Half-width of the BSA peak is equal ~15..20 mm.

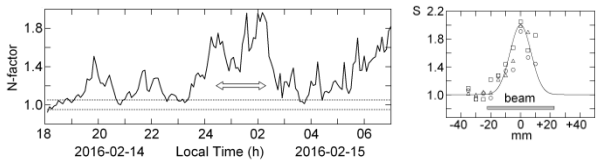

(a) (b)

Fig. 3. Temporal profile of the backscatter amplification factor *N* at a distance of 1900 m (a) and the normalized scanner signal *S* at the night (b) of February 14-15 of 2016 for three scans (○, □ and Δ) corresponding to the time interval on the left marked with an double arrow. The Gaussian approximation of experimental values is shown by the solid curve.

5. BSA-LIDAR vs. IMAGE JITTER SENSOR

In Fig. 4 the temporal profile of the amplification factor *N* for the same period as in Fig. 3a is compared with the root-mean-square (rms) deviation of the angular random displacements of the image energy centroid $\sigma=\sigma_c/F$. From Fig. 4 it is seen that the variations of the amplification *N*-factor correlate with the variations of σ. During our experiments the correlation coefficient was from 0.6 to 0.8. The temporal profile of the rms deviation σ is close to the variation of the amplification factor *N* in time. Thus, the value of the amplification factor depends on the refractive turbulence strength on the probing path.

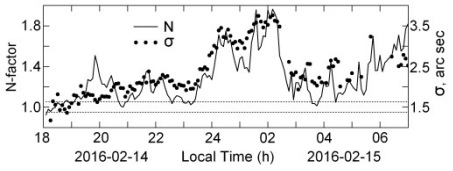

Fig. 4. Temporal variations of the amplification factor *N* at a distance of 1900 m (solid curve) and rms deviation of random image jitter σ (circles). Local time. Data of February 14-15 of 2016.

6. SPACE-TIME BSA-MAPPING

The function of the *N*-factor is a monotonic function with the positive first derivative [9,10]. If we differentiate this function, then the result is the rate of *N* increase along the sensing path. It allows represent the whole data array as a single range-time image of *dN/dz* (map). The derivative was determined from five values (*dz*=250 m). The procedure of the range-time mapping was applied to the data obtained on March 7 to 8 of 2016.

The data are depicted in Figure 5, and it consists of three parts. The figures show (a) integral values of the BSA factor *N* at the end of the 2-km sensing path, (b) standard deviation of the centroid of IJS disk image in arc seconds, and (c) range-time distribution of the derivative *dN/dz*. The depicted data reflect the dynamics of the process and allow to localize the areas with the weak and increased turbulence intensity.

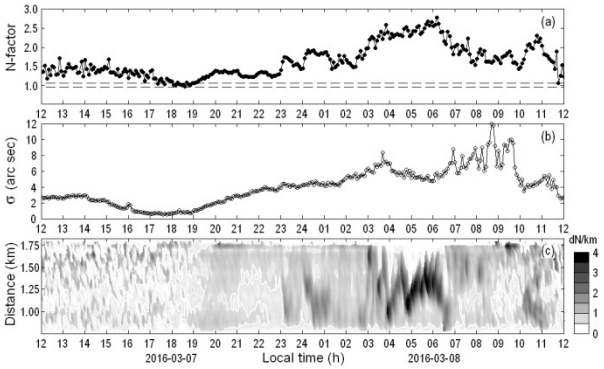

Fig. 5. Diurnal time series (a) of the integral backscatter amplification *N*-factor at a distance of 2 km, (b) variance of jitter of the disk image centroid at the 2-km path, and (c) range-time distribution of the derivative of the BSA factor. The correlation coefficient is equal to 0.65. Record from 12am of March 7 of 2016 to 12am of March 8 of 2016.

The comparison of the daytime and nighttime behavior of the *N*-factor shows that the space-time distribution is more homogeneous in the daytime, when the atmospheric temperature stratification is unstable. At 7 p.m. the neutral temperature stratification followed by the monotonic increase of the *N*-factor was observed. We observed the significant increase of the BSA factor in nighttime, which can be explained by appearance of significant temperature gradients.

The range-time distribution of *dN/dz* in Fig. 5c also allows us to explain the difference between the data of the BSA-lidar and the IJ-sensor, which

can be seen in Figs. 5a and 5b. The point is that the image jitter sensor recorded the maximal values of the variance near 8-9 a.m. (Fig. 5b), while the data of the BSA-lidar by this time decreased and showed the intensification at a level lower than two (Fig. 5a). If we refer to Fig. 5c, then we can see that by 7 a.m. the zone of intense turbulence became weaker and shifted toward the path end. However, for the IJ-sensor, just this section of the path is a major relative contributor to the sensor readings. Consequently, the discrepancy between the data of the BSA-lidar and the IJ-sensor is the caused by the inhomogeneous distribution of the turbulence intensity along the sensing path.

7. CONCLUSIONS

Thus, the paper has presented brief experimental results demonstrating the possibility of the BSA lidar measurement of the refractive turbulence strength averaged over the probing path. The incorporation of the third receiving channel into the BSA lidar has allowed us to obtain experimentally the profiles of the backscatter amplification factor over the receiving aperture.

The measured values of the amplification factor have been compared with the measured variance of random jitter of the optical image of the incoherent light source, which is directly proportional to the integral value of the structure constant of turbulent fluctuations of the refractive index of air on the probing path. The variations of the amplification factor in time are synchronous with the variations of the rms deviation of random image jitter. The high correlation between the amplification factor and the synchronously measured jitter rms deviation proves the possibility of lidar measurement of the refractive turbulence strength based on the effect of backscatter amplification.

Winter field lidar experiment in Tomsk city was carried out at the 2-km path to record the profile of the backscatter amplification coefficient. The differentiation of individual profiles of the BSA factor and drawing of their range-time image have allowed us to visualize the processes occurring in the atmosphere. It became possible to localize the zones with the increased turbulence intensity and to follow their temporal dynamics. The inhomogeneous emission of heat at night from heating of private houses leads to the smooth shift of turbulent zones, which can be followed remotely with the backscatter amplification lidar.

Under conditions of fine cloudless weather, the behavior of the BSA factor in daytime is quite predictable and correlates exactly with the amount of heat incoming to the surface. In the nighttime, the behavior of the BSA factor becomes hard to predict, because of a few different factors influencing turbulence in the air surface layer.

ACKNOWLEDGMENTS

The authors are grateful to A.S. Gurvich for initiation of the study, attention, and support, as well as to A.I. Nadeev for the help in design of instrumentation and consultations. Russian Scientific Foundation for Maintenance and Development, Agreement #14.607.21.0151.

REFERENCES

1. A.G. Vinogradov, Yu.A. Kravtsov, and V.I. Tatarskii, Radiophysics and Quantum Electronics **16**, 818 (1973).
2. A.S. Gurvich, and S.S. Kashkarov, Radiophysics and Quantum Electronics **20**, 547 (1977).
3. V. A. Banakh, and V.L. Mironov, *Lidar in a turbulent atmosphere* (Artech House. Boston & London. 1987. 185 p.)
4. A.S. Gurvich, Izvestiya, Atmospheric and Oceanic Physics **48**, 585 (2012).
5. V.A. Banakh, “Enhancement of the laser return mean power at the strong optical scintillation regime in a turbulent atmosphere”, Atmospheric and Oceanic Optics **26**, 90–95 (2013).
6. I.N. Smalikho, “Calculation of the backscatter amplification coefficient of laser radiation propagating in a turbulent atmosphere using numerical simulation”, Atmospheric and Oceanic Optics **26**, 135–139 (2013).
7. Yu.A. Kravtsov, A.I. Saichev, Physics-Uspekhi, **25**, 494 (1982).
8. I.A. Razenkov, V.A. Banakh, F.I. Nadeev. Russian Federation Patent No.153460, 2015.
9. V.A. Banakh, I.A. Razenkov, and I.N. Smalikho, Applied Optics, **54** (24), 7301 (2015).
10. V.A. Banakh and I.A. Razenkov. Optics Letters, **41** (19), 4429 (2016).
11. S. Manning, B.A. Clare, K.J. Grant, and K.A. Mudge, Optical Engineering **54** (11), 114104-1 (2015).